

Perspectives of e^+e^- production in pp, pd and pBe reactions at SIS energies

E. L. Bratkovskaya, W. Cassing, and U. Mosel

Institut für Theoretische Physik, Universität Gießen

35392 Gießen, Germany

Abstract

We study dilepton production from pp, pd and pBe collisions from 1 to 5 GeV including the ρ^0 , ω , ϕ and Dalitz decays, direct decays of vector mesons (ρ^0, ω) as well as subthreshold production via baryonic resonances (e.g. $D_{13}(1520); P_{11}(1710)$). Our calculations compare rather well with the pp and pd data from the DLS Collaboration, however, overestimate slightly the 'old' pBe data from that group. Furthermore, detailed predictions for differential dilepton spectra at SIS energies are made with a high mass resolution that can be controlled experimentally by the HADES Collaboration in near future.

PACS: 25.75Dw, 13.30Ce, 12.40Yx

Keywords: particle and resonance production; leptonic and semileptonic decays; hadron models

1 Introduction

Electromagnetic probes such as dileptons provide the most clear signals from the early phases of high-energy heavy-ion collisions because they may leave the reaction volume essentially undistorted by final-state interactions. Differential dilepton spectra from heavy-ion collisions thus can provide information about the effective degrees of freedom at high baryon density and temperature. Apart from that the in-medium properties of hadrons (cf. Refs. [1, 2, 3, 4, 5, 6]), that are closely related to the latter problem, can be explored as well. According to QCD sum rules [2, 5, 7] as well as QCD inspired effective Lagrangian models [1, 3, 4, 8, 9, 10, 11, 12, 13, 14] especially the vector mesons (ρ , ω and ϕ) significantly change their properties with nuclear density. It has been argued, that the experimentally observed enhanced production of soft lepton pairs above known sources in nucleus-nucleus collisions at SPS energies [15, 16] might be due to the in-medium modification of vector mesons [17, 18, 19, 20, 21] rather than reflecting a new state of hadronic matter.

Dileptons from heavy-ion collisions have also been measured by the DLS Collaboration [22, 23] at BEVALAC energies, where a different temperature and density regime is probed. The first generation of DLS data [22], based on a limited data set, were consistent with the results from early transport model calculations [24, 25, 26, 27] including the conventional dileptons sources as p-n bremsstrahlung, ρ^0 , ω , ϕ and Dalitz decay, direct decay of vector mesons and pion-pion annihilation, without incorporating any medium effects. A more recent DLS measurement [23] including the full data set and an improved analysis, however, shows an increase by about a factor of 5-7 in the cross section in comparison to Ref. [22] and the early theoretical predictions.

This enhancement of the e^+e^- yield in nucleus-nucleus collisions provides some theoretical 'puzzle'. In Ref. [28] the in-medium spectral functions from Refs. [13, 14] have been implemented in the HSD transport approach for mesons produced in baryon-baryon, pion-baryon collisions as well as from annihilation, and a factor of 2-3 enhancement has been obtained compared to the case of a free spectral function. In Ref. [29] dropping vector meson masses and ω meson broadening were incorporated in the URQM D transport model, which also showed an enhancement of the dilepton yield, however, the authors could not describe the new DLS data [23] as well. Another attempt to solve the DLS 'puzzle' has been performed in Ref. [30] where the dropping hadron mass scenario was considered together with the subthreshold production in N scattering via the baryonic resonance $N(1520)$ whose importance was pointed out in Refs. [14, 31]. It was found that the enhancement of the dilepton spectra due to low mass ω 's from the $N(1520)$ was not sufficient to match the DLS data. Thus, all in-medium scenarios that successfully have explained the dilepton enhancement at SPS energies failed to describe the new DLS dilepton data [23] from heavy-ion collisions ($^{12}\text{C} + ^{12}\text{C}$ and $^{40}\text{Ca} + ^{40}\text{Ca}$).

In 1998 the DLS Collaboration has, furthermore, published dilepton data from elementary pp and pd collisions at 1-5 GeV [32] which provides the possibility for an independent check of the elementary dilepton channels that enter as ‘input’ in transport calculations for heavy-ion reactions. Such an analysis has been carried out in Refs. [29, 33] and it was shown that the dilepton invariant mass spectra from pp reactions in the energy range from 1-5 GeV could be rather well described within the standard sources of hadronic Dalitz and direct decays when including also the ‘subthreshold’ production of mesons by baryonic resonances¹. It has been, furthermore, argued that additional channels (like dilepton decays of scalar mesons ($a_0; f_0$) or four-body final states decays like $\rho^0 \rightarrow \pi^+ e^+ e^-$, $(\rho^0; \omega) \rightarrow \pi^+ e^+ e^-$, $(\rho^0; \omega) \rightarrow \pi^0 e^+ e^-$) might contribute to the elementary yield in pp and pd reactions [34]. Thus it is indispensable, that also these elementary reactions have to be measured again with high resolution in order to understand more accurately the $e^+ e^-$ radiation mechanisms.

In this article we perform a detailed study of dilepton production from pp, pd and pBe collisions from 1-5 GeV including all channels as described in Ref. [33], i.e. the subthreshold production via baryonic resonances (e.g. $D_{13}(1520); P_{11}(1710)$) as well as ρ^0, ω, π^0 and Dalitz decays and the direct decay of vector mesons (ρ, ω, ϕ). We investigate the role of isospin degrees of freedom with respect to dilepton production in pd reactions by employing exact energy-momentum conservation for the deuteron target. The pBe reactions are calculated within the resonance transport model [35] that includes the same elementary production amplitudes.

The paper is organized as follows: In Section 2 we briefly present the underlying resonance model that enters the coupled-channel BUU transport approach. In Section 3 we provide a comparison of our results with the corresponding DLS data including the DLS acceptance and resolution functions. In Section 4 we, furthermore, give detailed predictions for these reactions with a high mass resolution in view of upcoming experiments with the HADES detector at GSI Darmstadt. We close with a summary and discussion of open problems in Section 5.

2 Description of the model

2.1 Resonance approach

We perform our analysis of dilepton production from pp, pd and pBe collisions within the resonance approach of Refs. [35, 36]. This model is based on the resonance concept of nucleon-nucleon and meson-nucleon interactions at low invariant energy \sqrt{s} [37] by adopting all resonance parameters from the Manley analysis [38]; all states with at least

¹For a detailed description of the individual channels we refer the reader to Ref. [33].

2 stars in Ref. [38] are taken into account: P_{33} (1232), P_{11} (1440), D_{13} (1520), S_{11} (1535), P_{33} (1600), S_{31} (1620), S_{11} (1650), D_{15} (1675), F_{15} (1680), P_{13} (1879), S_{31} (1900), F_{35} (1905), P_{31} (1910), D_{35} (1930), F_{37} (1950), F_{17} (1990), G_{17} (2190), D_{35} (2350). These resonances couple to the following channels: $N, N, N, K, (1232), N, N, N$ (1440), (1232) with respect to the production and decay.

It has been shown, that the resonance model provides a good description of the experimental data on one- and two-pion production in nucleon-nucleon collisions at low energy [37]. However, with increasing energy the resonance contributions underestimate the data; the missing yield is then treated as a background term to the resonance amplitude. This background term mimics t-channel particle production mechanism as well as other non-resonance contributions (e.g., direct $NN \rightarrow NN$, without creating an intermediate resonance).

With increasing energy, furthermore, the multiparticle production becomes more and more important. The high energy collisions { above $\sqrt{s} = 2.6$ GeV for baryon-baryon collisions and $\sqrt{s} = 2.2$ GeV for meson-baryon collisions } are described by the LUND string fragmentation model FRITIOF [39]. This aspect is similar to that used in the HSD approach [40, 20, 41, 42] and the URQMD model [43].

This combined resonance-string approach allows to calculate particle production in baryon-baryon and meson-baryon collisions from low to high energies. The collisional dynamics for proton-nucleus reactions, furthermore, is described by the coupled-channel BUU transport approach [35, 36] that is based on the same elementary cross sections.

2.2 Dilepton production

The dilepton production within the resonance model can be schematically presented in the following way:

$$BB \rightarrow R X \quad (1)$$

$$mB \rightarrow R X \quad (2)$$

$$R \rightarrow e^+ e^- X; \quad (3)$$

$$R \rightarrow m X; m \rightarrow e^+ e^- X; \quad (4)$$

$$R \rightarrow R^0 X; R^0 \rightarrow e^+ e^- X; \quad (5)$$

In words: in a first step a resonance R might be produced in baryon-baryon (BB) or meson-baryon (mB) collisions { (1), (2)}. Then this resonance can couple to dileptons directly { (3) (e.g., Dalitz decay of the resonance: $\rightarrow e^+ e^- N$) or decays to a meson (m + baryon) { (4) which produces dileptons via direct decays ($;!$) or Dalitz decays ($^0; ;!$). The resonance R might also decay into another resonance R^0 { (5) which later produces dileptons via Dalitz decay or again via meson decays (e.g., D_{35} (1930) !

to the ansatz used in the previous dilepton analysis [30, 33]. In Ref. [33] we have factorized the amplitude $\mathcal{N} \mathcal{N}^\dagger \mathcal{R} \mathcal{N}^\dagger \mathcal{N} \mathcal{N}^\dagger e^+ e^- \mathcal{N} \mathcal{N}^\dagger$ into a $D_{13}(1520)$ production part $(\mathcal{N} \mathcal{N}^\dagger \mathcal{R} \mathcal{N}^\dagger)$ and Dalitz decay part $\mathcal{R} \mathcal{N}^\dagger \mathcal{N} \mathcal{N}^\dagger e^+ e^- \mathcal{N}$ (cf. Sect. 3.1 of Ref. [33]). In the latter approach the ρ meson is considered to be on-shell, i.e. a virtual particle, and can have a mass below $2m_\rho$ which leads to the Dalitz behavior of the dilepton spectra (cf. Fig. 3 of Ref. [33]), whereas in the present approach we assume that the ρ meson has a free spectral function with masses only above $2m_\rho$. The latter assumption leads to the 'direct decay' profile for dileptons from subthreshold ρ 's and is consistent with our resonance prescription used also in the transport calculations [35], where we propagate such ρ mesons explicitly.

To compare with the experimental data of the DLS Collaboration one has to use the appropriate experimental filter, which is a function of the dilepton invariant mass M , transverse momentum p_T and rapidity y_{lab} in the laboratory frame $\{F(M; p_T; y_{lab})\}$. For that purpose we explicitly simulate all dileptons by Monte-Carlo and apply the filter $F(M; p_T; y_{lab})$.

3 $e^+ e^-$ results in comparison to DLS data

3.1 Dileptons from pp collisions

In Fig. 2 we present the calculated dilepton invariant mass spectra d^2N/dM^2 for pp collisions from 1.0 to 4.9 GeV including the natural mass resolution and filter $F(M; p_T; y_{lab})$ from the DLS Collaboration (version 4.1) in comparison to the DLS data [32]. The thin lines indicate the individual contributions from the different production channels; i.e. starting from low M : Dalitz decay $\rho^0 \rightarrow e^+ e^-$ (short dashed line), $\rho^\pm \rightarrow e^+ e^-$ (dotted line), $\rho^\pm \rightarrow N e^+ e^-$ (dashed line), $\rho^\pm \rightarrow \rho^0 e^+ e^-$ (dot-dashed line), for $M > 0.7$ GeV: $\rho^0 \rightarrow e^+ e^-$ (dot-dashed line), $\rho^\pm \rightarrow e^+ e^-$ (short dashed line). The full solid line represents the sum of all sources considered here.

Whereas at 1.04 GeV the dileptons stem practically all from ρ^0 and Dalitz decays, decay becomes more important with increasing energy and at high invariant mass. Note, that in the present analysis we do not separate the production mechanism for ρ mesons as in Ref. [33], i.e. the ρ -meson contribution might come from the decay of $D_{13}(1520)$ and $P_{11}(1710)$ or non-resonance production. Thus, the short dashed line (denoted as $\rho^0 \rightarrow e^+ e^-$) presents the sum of all contributions. However, the resonance mechanism dominates for production at low energies, especially below the pp \rightarrow pp threshold $\sqrt{s} < 2m_N + m_\rho$, where \sqrt{s} is the invariant collision energy (see Sec. 2 in Ref. [33]).

At 2.1 and 4.9 GeV the dilepton yield is dominated by the Dalitz decay and direct decays of ρ and ω mesons. The spectrum is enhanced towards low M due to the limited

phase space and strong mass dependence (M^{-3}) of the dilepton decay width [33] in line with the vector dominance model. Note, that at 2.1 GeV we use the resonance production mechanism in our model, whereas at 4.9 GeV most of the particles are produced by string decays. Within the strict resonance model which gives only the exclusive $pp \rightarrow pp$ cross section the yield from pp collisions is underestimated by about a factor of 2 (dot-dotted line) at 2.1 GeV. Since at this energy other channels such as $NN \rightarrow NN$ are open, we have estimated the cross section for these channels by the string model and added it to the total yield. This gives the final contribution (dotted line) for 2.1 GeV.

3.2 Dileptons from pd collisions

The experimental measurement of dilepton spectra from proton and deuteron targets provides a unique possibility to get information about the isospin dependence of the NN interaction which is interesting in itself and, furthermore, important with respect to heavy-ion reactions. The pp and pd dilepton data from the DLS Collaboration [32] are the first experimental step in this direction.

Since the deuteron is a bound system of proton and neutron, the Fermi motion of the nucleons plays an important role for all interactions. For example, Fermi motion leads to a shift of the threshold for particle production in pd interactions to lower $p_{\bar{s}}$, i.e. the channels closed by kinematics in pp collisions might be open in pd . Thus, the pd reactions can not be directly approximated by the simple sum of pp and pn . On the other hand, one can't treat the deuteron within the usual mean-field approach used in transport calculations for more heavy nuclei.

In our analysis we thus take into account the Fermi motion of nucleons using the momentum distribution of the deuteron calculated with the Paris potential [51]. We initialize a deuteron in momentum space (using a Monte Carlo method) according to the momentum distribution $f(p)$:

$$f(p) = \frac{j(p)j^2}{j(0)j^2}; \quad (7)$$

where p is the momentum of a nucleon in the deuteron center-of-mass, while $j(p)$ is the deuteron wave function. To fulfill the binding energy constraint we assume

$$E_{\text{spec}} = \sqrt{p^2 + m_N^2}; \quad E_{\text{part}} = E_d - E_{\text{spec}}; \quad (8)$$

The nucleon, which does not participate in the reaction, i.e. the spectator, has a free dispersion relation for the energy-momentum E_{spec} , whereas E_{part} is the energy of the nucleon participating in the reaction (participant). In (8) $E_d = 2m_N + B$ is the total deuteron energy, where $B = 2.2$ MeV is the binding energy of the deuteron.

The invariant collision-energy distribution $dN = d^3p_{\bar{s}}$ for pd reactions calculated with the dispersion relation (8) is shown by the solid histogram in Fig. 3. For comparison

(dashed histogram) we present the $dN = d^{\rho^-} \bar{s}$ distribution in the physical region ($2m_N < p_{\bar{s}} < p_{\bar{s}_{max}}$) calculated with $f(p)$ (7) in the quasi-free scattering limit, i.e. using the free dispersion relation for both nucleons in the deuteron: $E_{spec} = E_{part} = p^2 + m_N^2$. The lower limit of $p_{\bar{s}}$ is given by the free cross section that only exists for $p_{\bar{s}} > 2m_N$. As seen from Fig. 3, both prescriptions are the same in the peak value, however, the deuteron spectral distribution (8) leads to an enhancement of the $p_{\bar{s}}$ distribution at small $p_{\bar{s}}$ and a reduction at high $p_{\bar{s}}$. This implies a substantial lowering of particle production at high $p_{\bar{s}}$ with respect to the quasi-free limit, which has been often used in the literature.

Within the 'binding' prescription (8) we have calculated the dilepton invariant mass spectra d^2M for pd collisions from 1.0 to 4.9 GeV including the natural mass resolution and $d^2F(M; p_T; y_{lab})$ from the DLS Collaboration (version 4.1). The results are shown in Fig. 4 in comparison to the DLS data [32], where the assignment of the lines is the same as in Fig. 2. Additionally, the dot-dot-dashed lines indicate the pn bremsstrahlung contributions.

Similar to Fig. 2, at 1.04 GeV the ρ^0 and Dalitz decays are dominant, however, due to the larger mass of the deuteron, the ω channel is already open contrary to the pp reaction and the subthreshold ω branch is getting more important at high invariant mass M . Also pn bremsstrahlung contributes at low energies, however, with increasing bombarding energy it becomes less important.

Starting from 1.61 GeV the dominant contribution at low M is again the Dalitz decay, whereas at high M the dileptons stem basically from direct ρ^0 decays. The contribution here is calculated by assuming $\rho_{pn}^+ \rho_{pn}^- = 6 \rho_{pp}^+ \rho_{pp}^-$ for $2.425 \text{ GeV} < p_{\bar{s}} < 2.517 \text{ GeV}$ in line with the experimental data from Ref. [52], $\rho_{pn}^+ \rho_{pn}^- = 2.5 \rho_{pp}^+ \rho_{pp}^-$ for $2.517 \text{ GeV} < p_{\bar{s}} < 2.65 \text{ GeV}$ and $\rho_{pn}^+ \rho_{pn}^- = \rho_{pp}^+ \rho_{pp}^-$ for $p_{\bar{s}} > 2.65 \text{ GeV}$ where the multiparticle production (above 2.65 GeV) is evaluated within the LUND string model. Note, that at high $p_{\bar{s}}$ the isospin asymmetry $\rho_{pn}^+ = \rho_{pp}^+$ should be washed out by the isospin of pions that are created together with the ρ . Though this 'recipe' seems to work in comparison to the DLS data, we point out that further experimental data with good mass resolution will be necessary to clarify the situation for the isospin couplings.

In order to demonstrate the importance of isospin degrees-of-freedom for dilepton production we present in Fig. 5 the invariant mass spectra d^2M for pp (short dashed line), pn (long dashed line), pp+pn (dot-dashed line) and pd (solid line) collisions at 1.61 GeV in comparison to the DLS data [32]. At these energies the pn channel gives the main contribution to the pd dilepton yield. Furthermore, the influence of the Fermi motion in the deuteron is clearly seen at high invariant mass M by comparing the dot-dashed (pp+pn) and solid (pd) lines.

In Fig. 6 we present the excitation function, i.e. the integrated dilepton cross section for masses above 0.15 GeV, as a function of the available energy $Q = p_{\bar{s}} - 2m_p$ for pp

(dashed line) and pd (solid line) in comparison to the DLS data [32] (open circles for pp and full circles for pd). The calculated excitation functions for pp and pd increase with the energy and stay within the experimental errorbars.

3.3 Dileptons from pBe collisions

Since Be is one of the lightest nuclei, in-medium effects play a minor role because most hadron decays occur already in vacuum. So one can consider pBe collisions as an additional and independent check for the elementary reactions and isospin degrees of freedom. However, the collisional dynamics has to be taken into account properly. For that purpose we use the coupled-channel BUU transport approach as discussed in Sec. 2.

Dileptons from pBe have been measured by the DLS Collaboration in the end of the 80's [22]. In Fig. 7 we show the calculated dilepton invariant mass spectra d^2N/dM^2 for pBe collisions at 1.0 (upper part), 2.1 (middle part) and 4.9 GeV (lower part) including the natural mass resolution and filter $F(M; p_T; y_{lab})$ from the DLS Collaboration (version 1.6) in comparison to the data [22]. The assignment of the lines is the same as in Figs. 2 and 4. With the filter 1.6 we do not get enough suppression for the dilepton yield at $M = 0.15$ GeV which basically stems from 0 Dalitz decay. Similar to pd reactions the dominant channels at 1.0 GeV are the Dalitz decay and pn bremsstrahlung. At 2.1 and 4.9 GeV the Dalitz decay becomes important at low M and the direct decays of vector mesons ($\rho; \omega$) for $M = 0.8$ GeV. Within the present model we slightly overestimate the data at 4.9 GeV, however, we discard any discussion about the physical reason since the 'old' DLS filter is not sufficiently understood. For example, the 'old' DLS data for pBe at 4.9 GeV show a similar dilepton yield as for pd, whereas according to our calculations it should be higher by a factor of ~ 2 since more nucleons are involved in the pBe reaction.

In this respect we have performed detailed calculations for pp, pd and pBe reactions without implementing any filter, however, including a high (10 MeV) mass resolution for d^2N/dM^2 . For the results, that can be controlled by the HADES Collaboration in near future, we refer to the following Section.

4 Predictions for HADES

In this Section we present our predictions for the dilepton invariant mass spectra, transverse momentum (p_T) distributions and rapidity (y) distributions for pp, pd and pBe collisions at 1.5 GeV and 4.0 GeV, which will be measured with the HADES spectrometer at GSI.

In Fig. 8 the calculated dilepton invariant mass spectra d^2N/dM^2 for pp (upper part), pd (middle part) and pBe collisions (lower part) at 1.5 GeV (left panel) and 4.0 GeV

(right panel) are shown including a $M = 10 \text{ MeV}$ mass resolution. The assignment of the lines is the same as in Figs. 2 and 4. The dominant contribution at low M ($> m_\rho$) is the ρ Dalitz decay, however, for $M > 0.4 \text{ GeV}$ the dileptons stem basically all from direct vector meson decays (ω and ρ). With a 10 MeV mass resolution the peak from the direct ρ decay (which was completely smeared out within the DLS mass resolution) is seen. The ρ peak is getting more pronounced at high energy (cf. the right panel of Fig. 8).

In Fig. 9 we present the transverse momentum distribution $d^2N/dp_T^2 = (2\pi p_T)^{-1}$ for pp (upper part), pd (middle part) and pBe collisions (lower part) at 1.5 GeV (left panel) and 4.0 GeV (right panel). The assignment of the lines again is the same as in Figs. 2 and 4. Here we did not imply any cut in the invariant mass M . For all systems and energies considered the ρ Dalitz decay is much higher than all other contributions, which is in line with the result of Fig. 8 because the pion production cross section is much larger than that for the other mesons. The shape of the ρ ; ω ; ρ ! Dalitz decays is defined by the kinematics of the Dalitz decay and the 'at' part at low p_T depends on the mass of the decaying resonance.

The laboratory rapidity distributions dN/dy for pp (upper part), pd (middle part) and pBe collisions (lower part) at 1.5 GeV (left panel) and 4.0 GeV (right panel) are shown in Fig. 10, where the assignment of the lines is the same as before. The situation is similar to Fig. 9, { the ρ Dalitz decay is the only visible contribution when imposing no cuts on the invariant mass.

In order to make the contribution from other channels visible one has to suppress the 'background' ρ yield. In Fig. 11 we display the transverse momentum spectra for pp (upper part), pd (middle part) and pBe collisions (lower part) at 1.5 GeV (left panel) and 4.0 GeV (right panel) using a cut in invariant mass as $0.4 \text{ GeV} < M < 0.7 \text{ GeV}$. Fig. 12 shows the laboratory rapidity distributions for the same systems and kinematical conditions. With this cut on intermediate dilepton masses one can select the region where the ρ Dalitz decay is totally removed and the ω Dalitz decay is suppressed substantially (cf. Fig. 8); in this way the ω branch in the transverse momentum and rapidity spectra becomes seen (cf. Figs. 10, 11). Thus, a measurement of the transverse momentum and rapidity spectra with a corresponding cut in M will provide additional and independent information about the ω contribution to the dilepton spectra.

Finally, in Fig. 13 we present the double differential dilepton spectra $d^2N/dM dp_T$ as a function of the invariant mass M and transverse momentum p_T for pd collisions at 4.0 GeV . At fixed p_T one can recognize the shape of the invariant mass spectra (cf. Fig. 8) with a strong ρ Dalitz decay branch at low M as well as the contributions from ω Dalitz decay and the vector meson (ω ; ρ) decays. At fixed M the shape looks similar to the one in Fig. 9. At low M the exponential decrease stems from ρ Dalitz decay, then the

spectra become flatter due to the contributions from Dalitz ($M < 0.4 \text{ GeV}$) and direct decays. At $M = 0.78 \text{ GeV}$ the peak from the direct decay of ρ mesons is visible. Thus, such type of 3-dimensional experimental information (or even 4-dimensional including rapidity) allows to select the contributions from different channels.

5 Summary

Within the framework of the combined resonance-string approach we have performed a detailed study of dilepton production from pp, pd and pBe collisions at 1.0 { 4.9 GeV. In this approach the particle production proceeds through resonances at low energies and by string formation and decay at high energies. The collisional dynamics is described by the coupled-channel BUU transport approach. As dilepton sources we have considered ρ^0 , ω , ρ^\pm and Dalitz decays, pn bremsstrahlung and direct decays of vector mesons (ρ , ω).

We have compared our calculated results to the experimental data of the DLS Collaboration which provide constraints on the different individual production channels. It has been found that the DLS data for the pp and pd collisions can be reasonably well described in our model whereas for pBe systems (especially at 4.9 GeV) our calculations give a slightly higher dilepton yield. We have demonstrated the importance to measure the dileptons from pp and pd (or even pBe) collisions simultaneously since such data can provide constraints on the isospin dependence of pp and pn interactions, which is important for an understanding of heavy-ion data.

Dilepton spectra from elementary reactions will be measured in future by the HADES detector at GSI Darmstadt with high mass resolution and good accuracy. In this respect we have made predictions for the dilepton invariant mass spectra, transverse momentum and rapidity distributions for pp, pd and pBe at 1.5 and 4.0 GeV. We showed that proper cuts in invariant mass for transverse momentum and rapidity spectra allow to select different dilepton sources and to study, for example, the ρ meson channel in more detail. We have indicated, furthermore, that it might be very useful to provide experimentally multi-dimensional information, e.g. double differential dilepton spectra $d^2N/dM dp_T$, in order to investigate the individual contributions.

Acknowledgements

The authors are grateful for valuable discussions with J. Friese, M. Kagarlis and A. Sibirtsev.

References

- [1] G. E. Brown and M. Rho, *Phys. Rev. Lett.* 66 (1991) 2720.
- [2] T. Hatsuda and S. Lee, *Phys. Rev. C* 46 (1992) R34.
- [3] C. M. Shakin and W. D. Sun, *Phys. Rev. C* 49 (1994) 1185.
- [4] F. Klingl and W. Weise, *Nucl. Phys. A* 606 (1996) 329; F. Klingl, N. Kaiser and W. Weise, *Nucl. Phys. A* 624 (1997) 527.
- [5] M. Asakawa and C. M. Ko, *Phys. Rev. C* 48 (1993) R526.
- [6] U. Mosel, *Ann. Rev. Nucl. Part. Sci.* 41 (1991) 29.
- [7] S. Leupold, W. Peters and U. Mosel, *Nucl. Phys. A* 628 (1998) 311.
- [8] M. Hermann, B. Friman, and W. Norenberg, *Nucl. Phys. A* 560 (1993) 411.
- [9] M. Asakawa, C. M. Ko, P. Levai, and X. J. Qu, *Phys. Rev. C* 46 (1992) R1159.
- [10] G. Chanfray and P. Schuck, *Nucl. Phys. A* 545 (1992) 271c.
- [11] R. Rapp, G. Chanfray, and J. Wambach, *Phys. Rev. Lett.* 76 (1996) 368.
- [12] B. Friman and H. J. Pinner, *Nucl. Phys. A* 617 (1997) 496.
- [13] R. Rapp, G. Chanfray and J. Wambach, *Nucl. Phys. A* 617 (1997) 472.
- [14] W. Peters, M. Post, H. Lenske, S. Leupold, and U. Mosel, *Nucl. Phys. A* 632 (1998) 109.
- [15] G. Agakichiev et al., *Phys. Rev. Lett.* 75 (1995) 1272; Th. Ullrich et al., *Nucl. Phys. A* 610 (1996) 317c; A. Drees, *Nucl. Phys. A* 610 (1996) 536c.
- [16] M. A. Mazoni, *Nucl. Phys. A* 566 (1994) 95c; M. Maseara, *Nucl. Phys. A* 590 (1995) 93c; T. Akeesson et al., *Z. Phys. C* 68 (1995) 47.
- [17] G. Q. Li, C. M. Ko, and G. E. Brown, *Phys. Rev. Lett.* 75 (1995) 4007.
- [18] C. M. Ko, G. Q. Li, G. E. Brown, and H. Sorge, *Nucl. Phys. A* 610 (1996) 342c.
- [19] W. Cassing, W. Ehehalt, and C. M. Ko, *Phys. Lett. B* 363 (1995) 35; W. Cassing, W. Ehehalt, and I. Kralik, *Phys. Lett. B* 377 (1996) 5.
- [20] E. L. Bratkovskaya and W. Cassing, *Nucl. Phys. A* 619 (1997) 413.
- [21] W. Cassing, E. L. Bratkovskaya, R. Rapp, and J. Wambach, *Phys. Rev. C* 57 (1998) 916.

- [22] G .Roche et al, Phys. Rev. Lett. 61 (1988) 1069; C .Naudet et al, Phys. Rev. Lett. 62 (1989) 2652; G .Roche et al, Phys. Lett. B 226 (1989) 228.
- [23] R .J .Porter et al, Phys. Rev. Lett. 79 (1997) 1229.
- [24] L .Xiong, Z .G .Wu, C .M .Ko, and J .Q .Wu, Nucl. Phys. A 512 (1990) 772.
- [25] G y .W olf, G .Batko, W .Cassing, U .M osel, K .Niita, and M .Schafer, Nucl. Phys. A 517 (1990) 615; G y .W olf, W .Cassing and U .M osel, Nucl. Phys. A 552 (1993) 549.
- [26] K K .Gudima, A .I .Titov and V D .Toneev, Sov. Jour. of Nucl. Phys. 55 (1992) 1715.
- [27] E .L .B ratkovskaya, W .Cassing and U .M osel, Phys. Lett. B 376 (1996) 12.
- [28] E .L .B ratkovskaya, W .Cassing, R .Rapp, and J .W ambach, Nucl. Phys. A 634 (1998) 168.
- [29] C .Emst, S .A .Bass, M .Belkacem, H .Stocker, and W .Greiner, Phys. Rev. C 58 (1998) 447.
- [30] E .L .B ratkovskaya and C M .Ko, Phys. Lett. B 445 (1999) 265.
- [31] G .E .Brown, G .Q .Li, R .Rapp, M .Rho, and J .W ambach, Acta Phys. Polon. B 29 (1998) 2309.
- [32] W K .Wilson et al, Phys. Rev. C 57 (1998) 1865.
- [33] E .L .B ratkovskaya, W .Cassing, M .E enberger, U .M osel, Nucl. Phys. A 653 (1999) 301.
- [34] A .Faessler, C .Fuchs and M .I .K rivosuchenko, Phys. Rev. C 61 (2000) 035206.
- [35] M .E enberger, E .B ratkovskaya and U .M osel, Phys. Rev. C 60 (1999) 044614.
- [36] M .E enberger, Ph.D . Thesis, Univ. of G iessen, 1999; <http://theorie.physik.uni-giessen.de/ftp.html>.
- [37] S .Teis, W .Cassing, M .E enberger, A .Hom bach, U .M osel, and G y .W olf, Z .Phys. A 356 (1997) 421; Z .Phys. A 359 (1997) 297.
- [38] D M .Manley and E M .Saleski, Phys. Rev. D 45 (1992) 4002.
- [39] B .Anderson, G .Gustafson and H ong Pi, Z .Phys. C 57 (1993) 485.
- [40] W .Ehehalt and W .Cassing, Nucl. Phys. A 602 (1996) 449.
- [41] J .Geiss, W .Cassing, and C .Greiner, Nucl. Phys. A 644 (1998) 107.

- [42] W .Cassing and E .L .B ratkovskaya, Phys. Rep. 308 (1999) 65.
- [43] S .A .B ass et al, Prog. Part. Nucl. Phys. 42 (1998) 279; J. Phys. G 25 (1999) 1859.
- [44] C .G ale and J. K apusta, Phys. Rev. C 35 (1987) 2107; C 40 (1987) 2397.
- [45] C .G ale and J. K apusta, Nucl. Phys. A 495 (1989) 423c.
- [46] M .Schafer, T .S .B iro, W .Cassing, and U .M osel, Phys. Lett. B 221 (1989) 1.
- [47] M .Schafer, H .C .D onges, A .Engel and U .M osel, Nucl. Phys. A 575 (1994) 429.
- [48] A .I .T itov, B .K am pfer and E .L .B ratkovskaya, Phys. Rev. C 51 (1995) 227.
- [49] F .de Jong and U .M osel, Phys. Lett. B 379 (1996) 45; B 392 (1997) 273.
- [50] E .L .B ratkovskaya, W .Cassing, L .A .K ondratyuk, and A .S ibirtsev, Eur. Phys. J. A 4 (1999) 165.
- [51] M .Lacombe et al, Phys. Lett. B 101 (1981) 139.
- [52] E .Chiavassa et al, Phys. Lett. B 322 (1994) 270; B 337 (1994) 192; H .C alen et al, Phys. Rev. C 58 (1998) 2667.

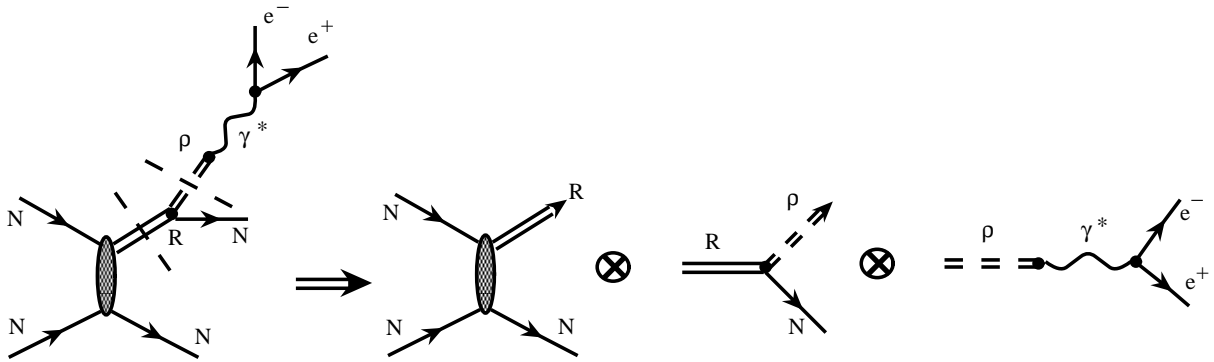


Figure 1: Factorization of the diagram for the process $NN \rightarrow RN \rightarrow NN \rightarrow e^+e^- NN$ with an intermediate baryon resonance R .

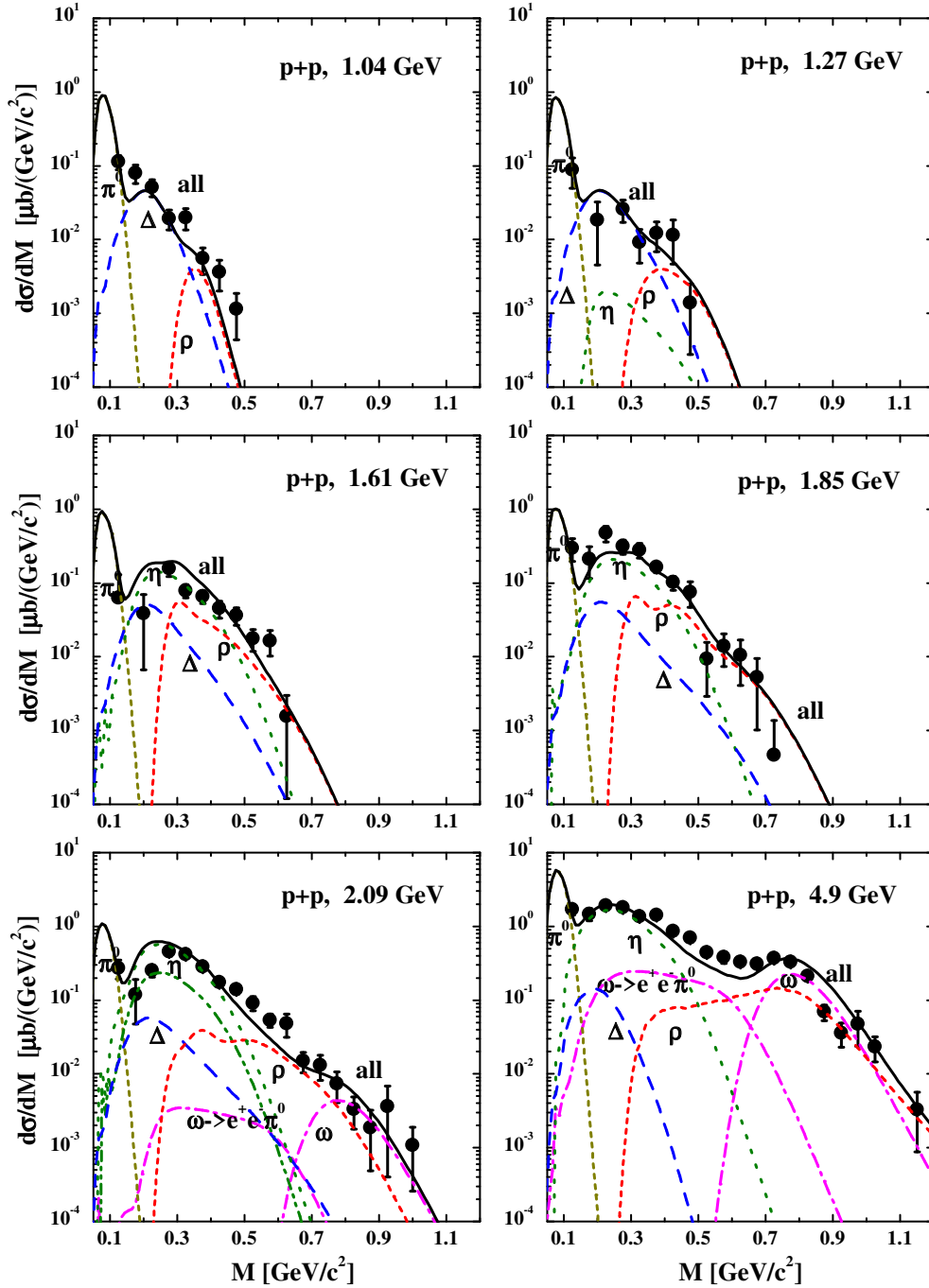


Figure 2: The calculated dilepton invariant mass spectra $d\sigma/dM$ for pp collisions from 1.0 { 4.9 GeV in comparison to the DLS data [32]. The thin lines indicate the individual contributions from the different production channels; i.e. starting from low M : Dalitz decay $\rho^0 \rightarrow e^+e^-$ (short dashed line), $\Delta \rightarrow e^+e^-$ (dotted line), $\eta \rightarrow e^+e^-$ (dashed line), $\pi \rightarrow e^+e^-$ (dot-dashed line); for $M > 0.7$ GeV: $\omega \rightarrow e^+e^-$ (dot-dashed line), $\omega \rightarrow e^+e^- \pi^0$ (short dashed line). The full solid line represents the sum of all sources considered here. At 2.09 GeV the dot-dot-dashed line indicates the contribution from the resonance decays only while the dotted line corresponds to the inclusive production (see text).

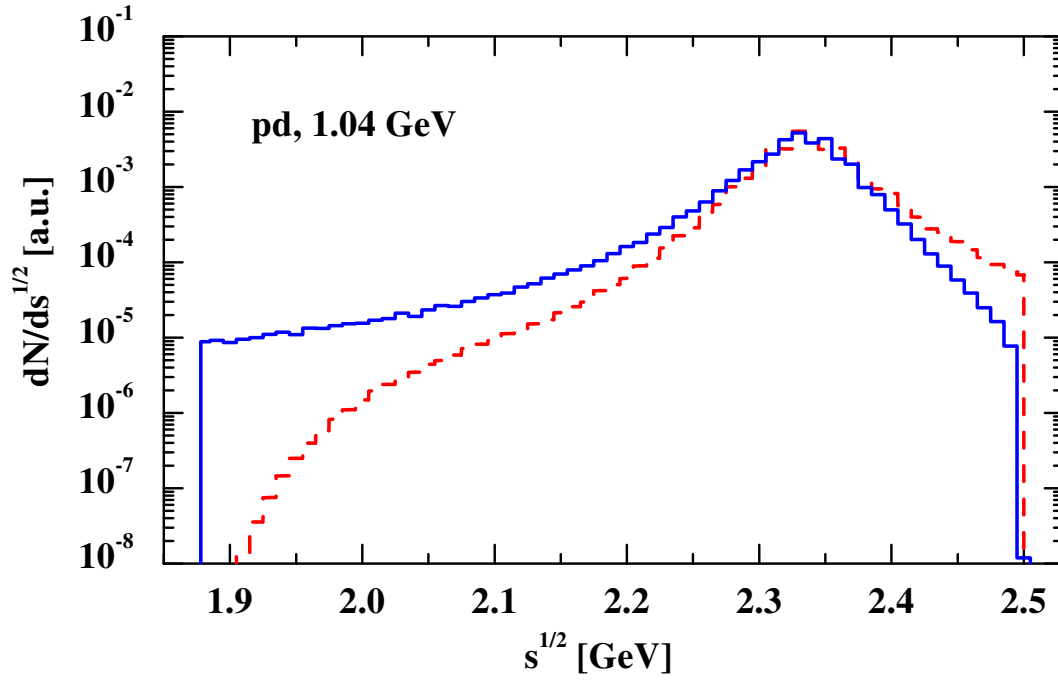


Figure 3: The distribution in the invariant collision energy \sqrt{s} ($dN = d\sqrt{s}$) in arbitrary units for the pd reaction at 1.04 GeV calculated with the dispersion relation (8) (solid histogram) and within the quasi-free scattering limit (dashed histogram).

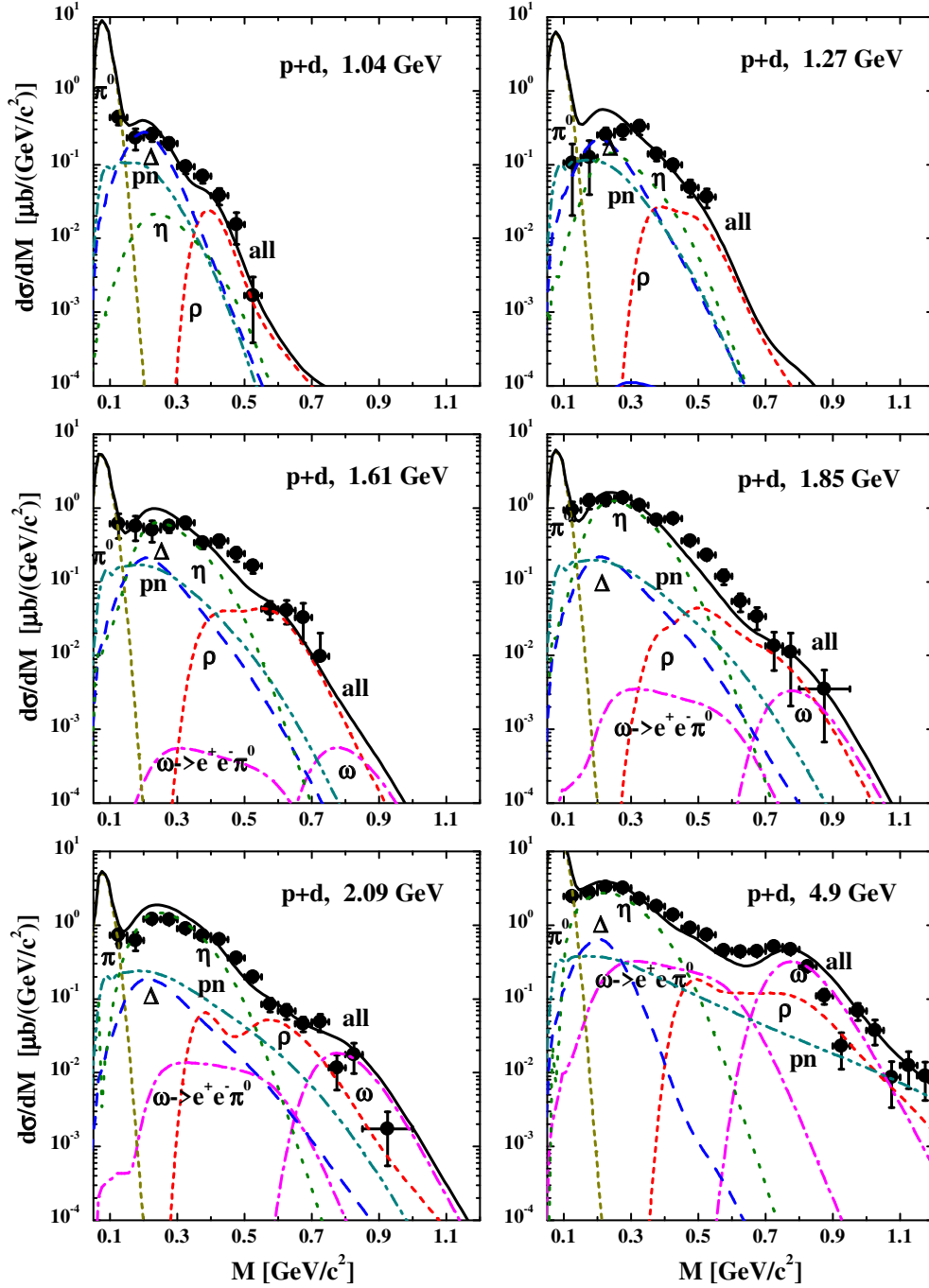


Figure 4: The dilepton invariant mass spectra $d\sigma/dM$ for pd collisions from 1.0 to 4.9 GeV in comparison to the DLS data [32]. The assignment of the lines is the same as in Fig. 2. Additionally, the dot-dot-dashed lines indicate the pn bremsstrahlung contributions.

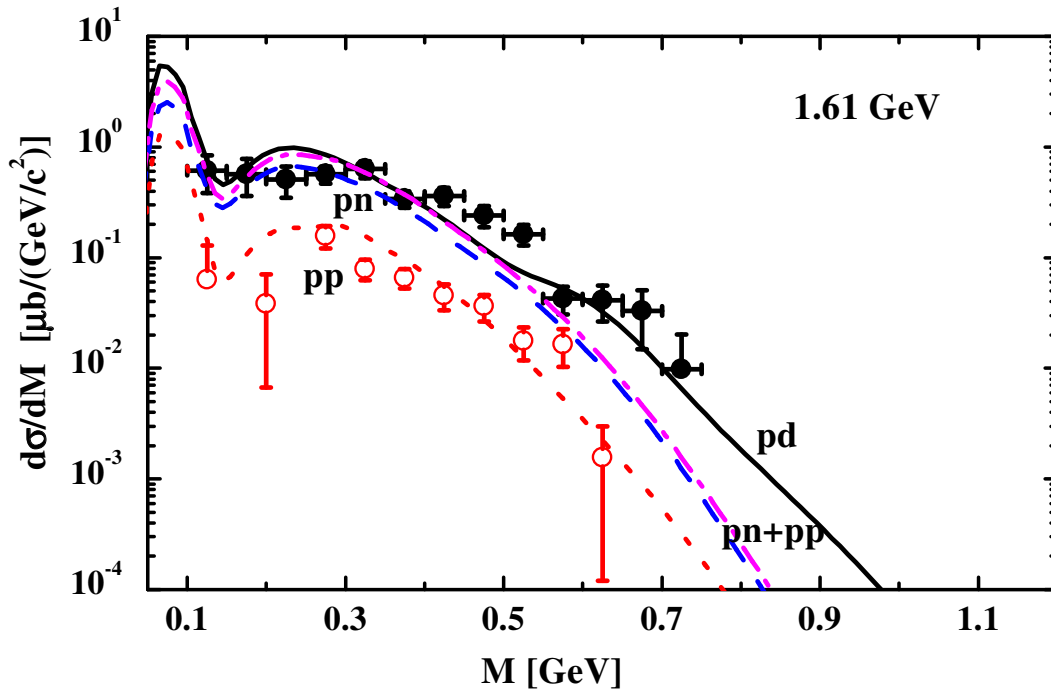


Figure 5: The dilepton invariant mass spectra $d\sigma/dM$ for pp (short dashed line), pn (long dashed line), pp + pn (dot-dashed line) and pd (solid line) collisions at 1.61 GeV in comparison to the DLS data [32]. The difference between the dot-dashed line and the solid line stems from the Fermi motion of the nucleons in the deuteron.

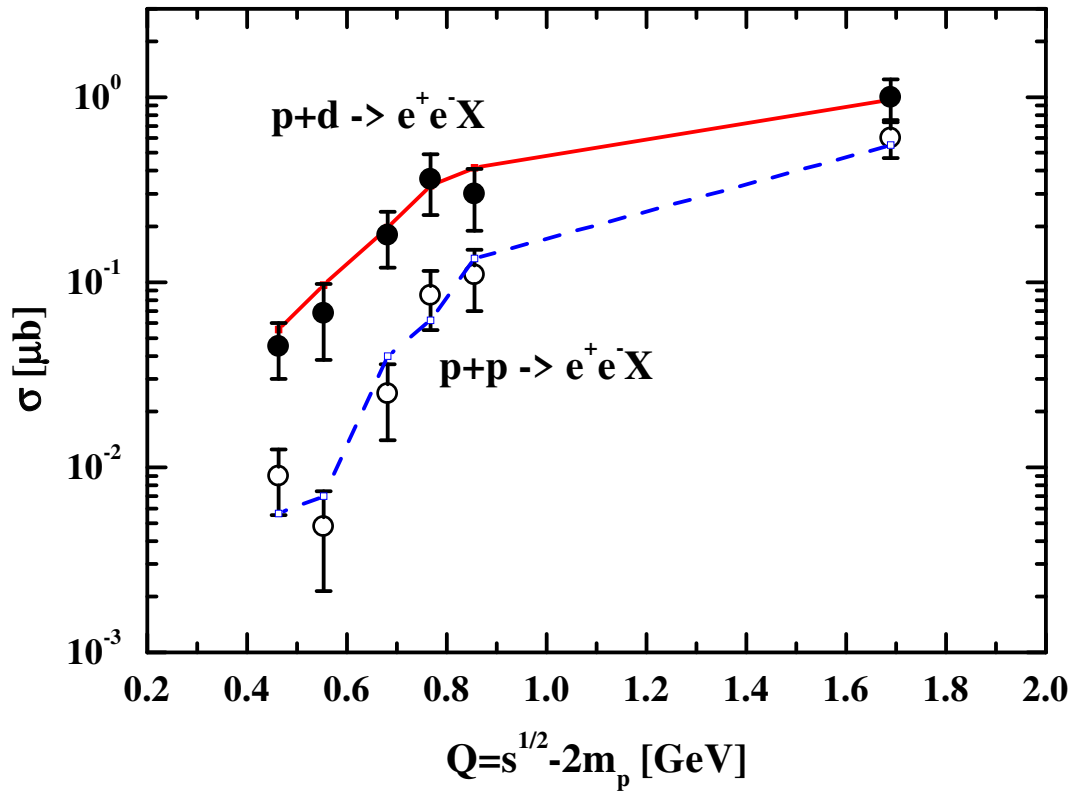


Figure 6: The excitation function for dileptons from pp (dashed line) and pd (solid line) in comparison to the DLS data [32] (open circles for pp and full circles for pd reactions).

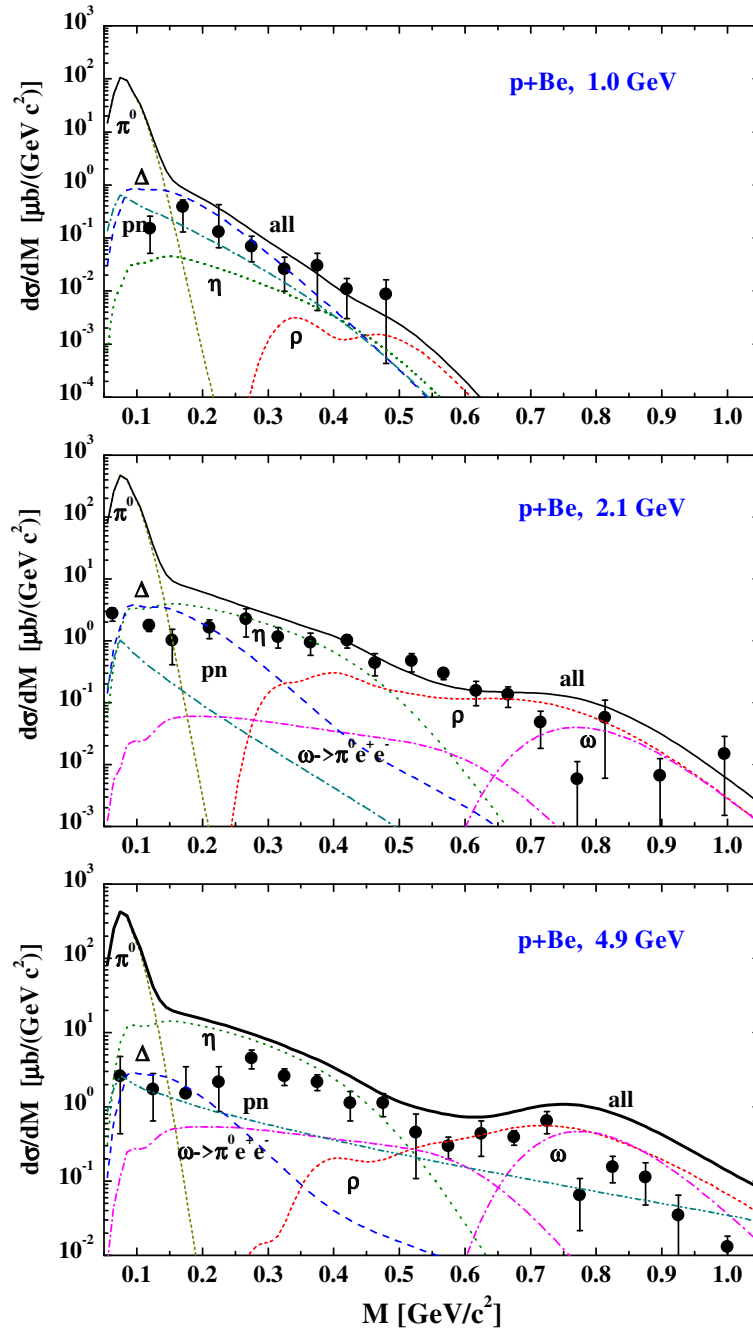


Figure 7: The dilepton invariant mass spectra $d\sigma/dM$ for pBe collisions at 1.0 GeV (upper part), 2.1 GeV (middle part) and 4.9 GeV (lower part) in comparison to the DLS data [22]. The assignment of the individual lines is the same as in Figs. 2, 4.

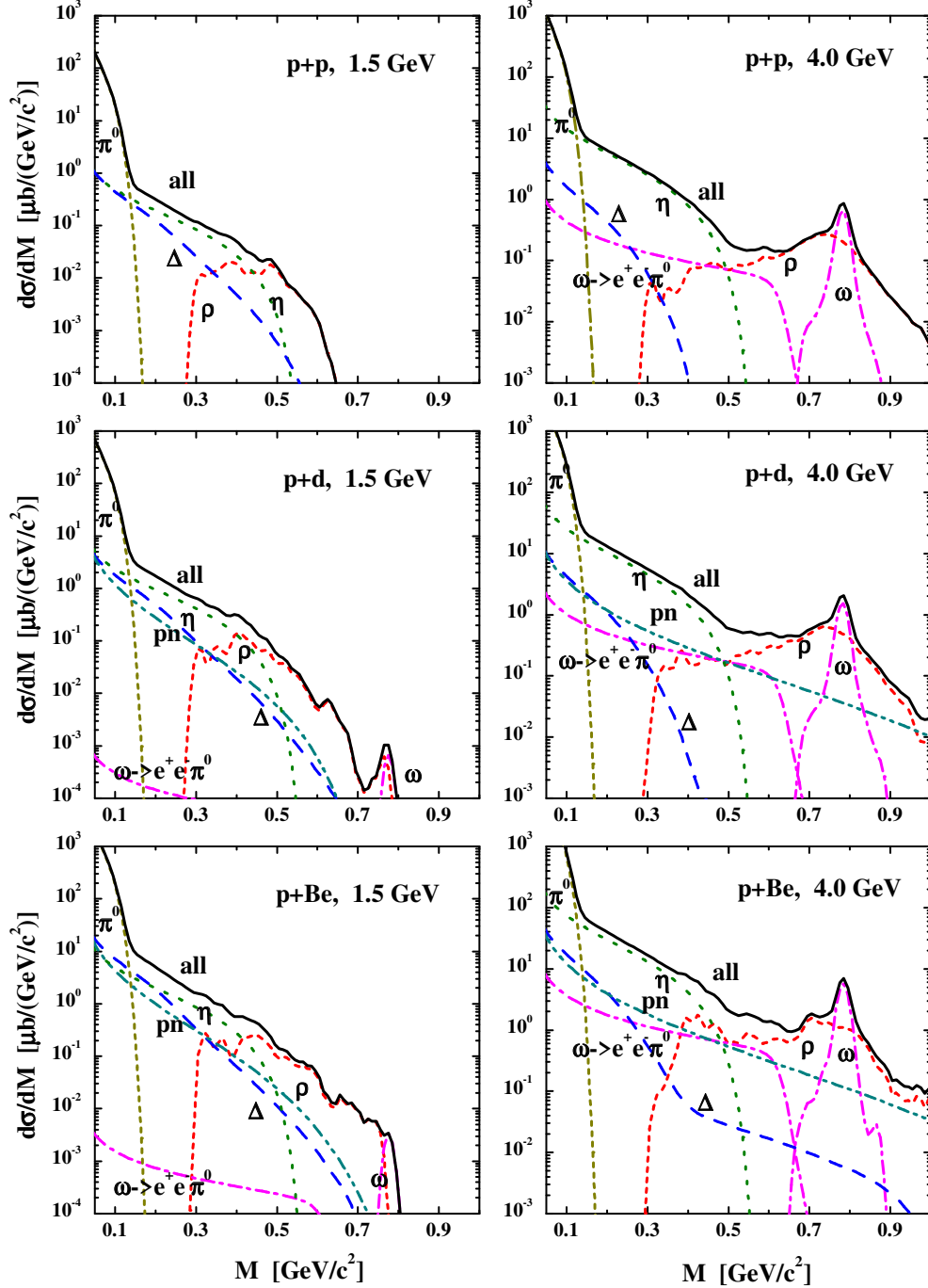


Figure 8: The dilepton invariant mass spectra $d\sigma/dM$ for pp (upper part), pd (middle part) and pBe collisions (lower part) at 1.5 GeV (left panel) and 4.0 GeV (right panel) including a 10 MeV mass resolution. The assignment of the individual lines is the same as in Figs. 2, 4.

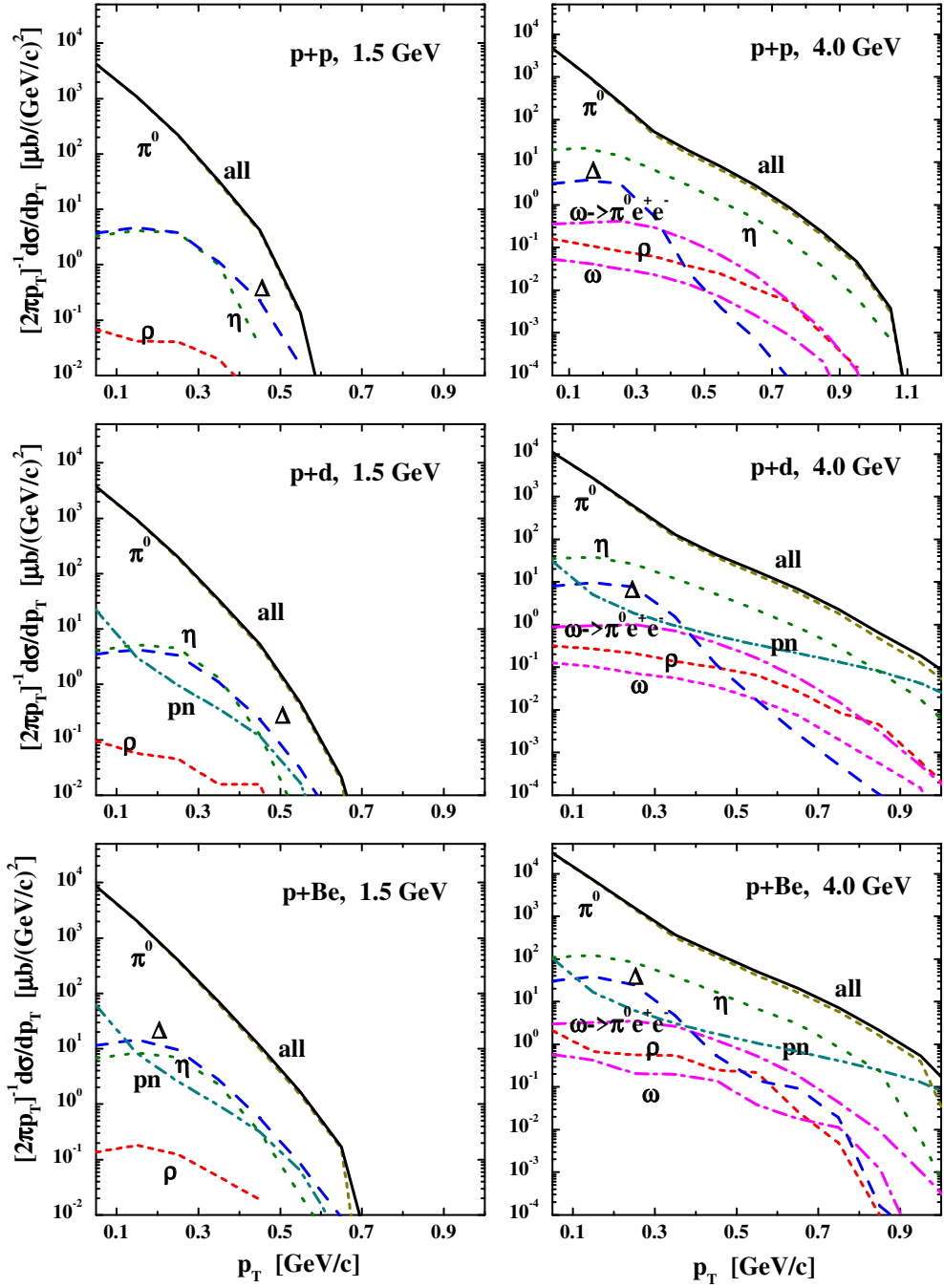


Figure 9: The transverse momentum distribution $d\sigma/dp_T = (2\pi p_T)^{-1} d\sigma/dp_T$ for pp (upper part), pd (middle part) and pBe collisions (lower part) at 1.5 GeV (left panel) and 4.0 GeV (right panel). The assignment of the individual lines is the same as in Figs. 2, 4.

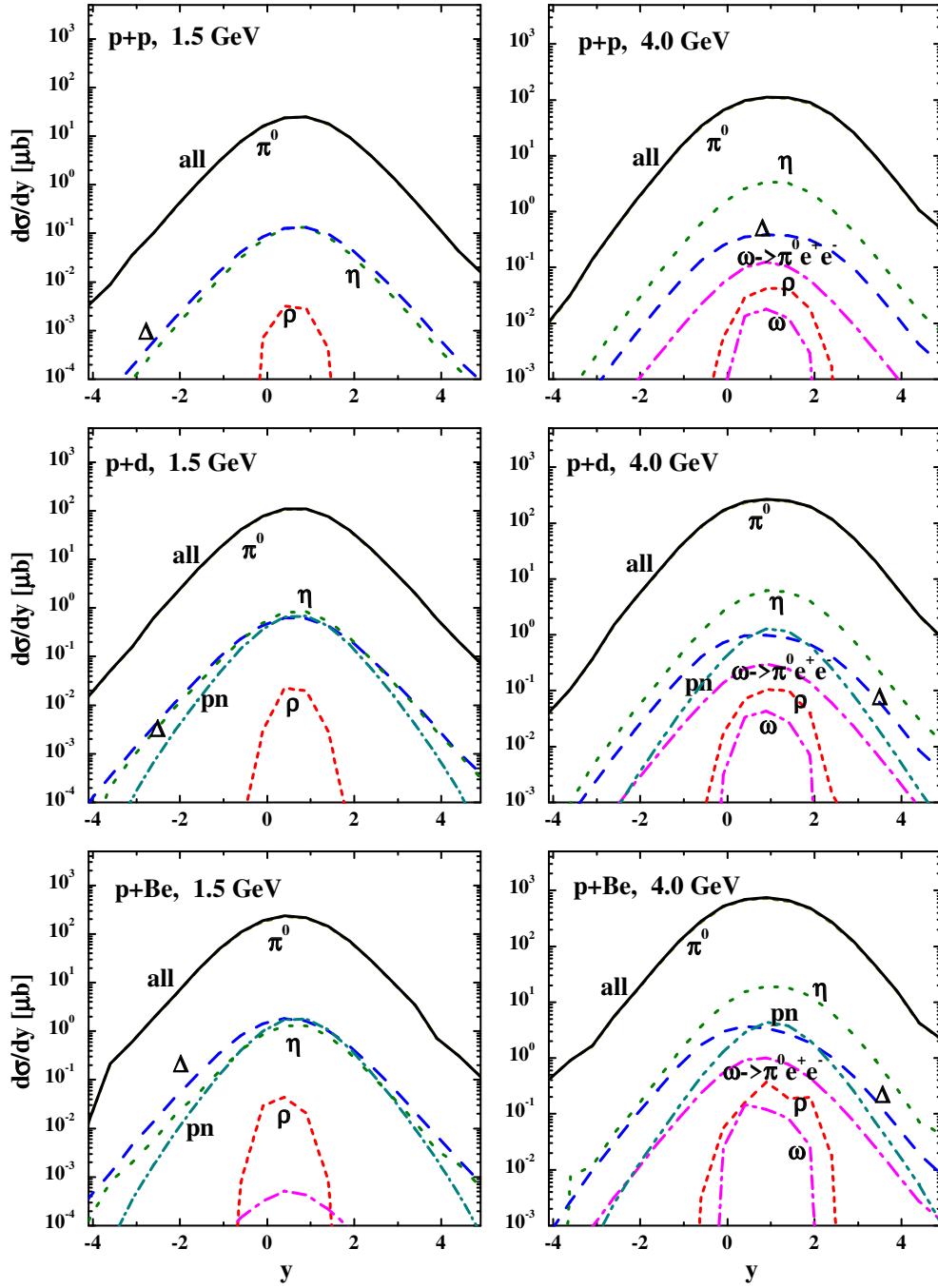


Figure 10: The rapidity distributions $d\sigma/dy$ for pp (upper part), pd (middle part) and pBe collisions (lower part) at 1.5 GeV (left panel) and 4.0 GeV (right panel). The assignment of the individual lines is the same as in Figs. 2, 4.

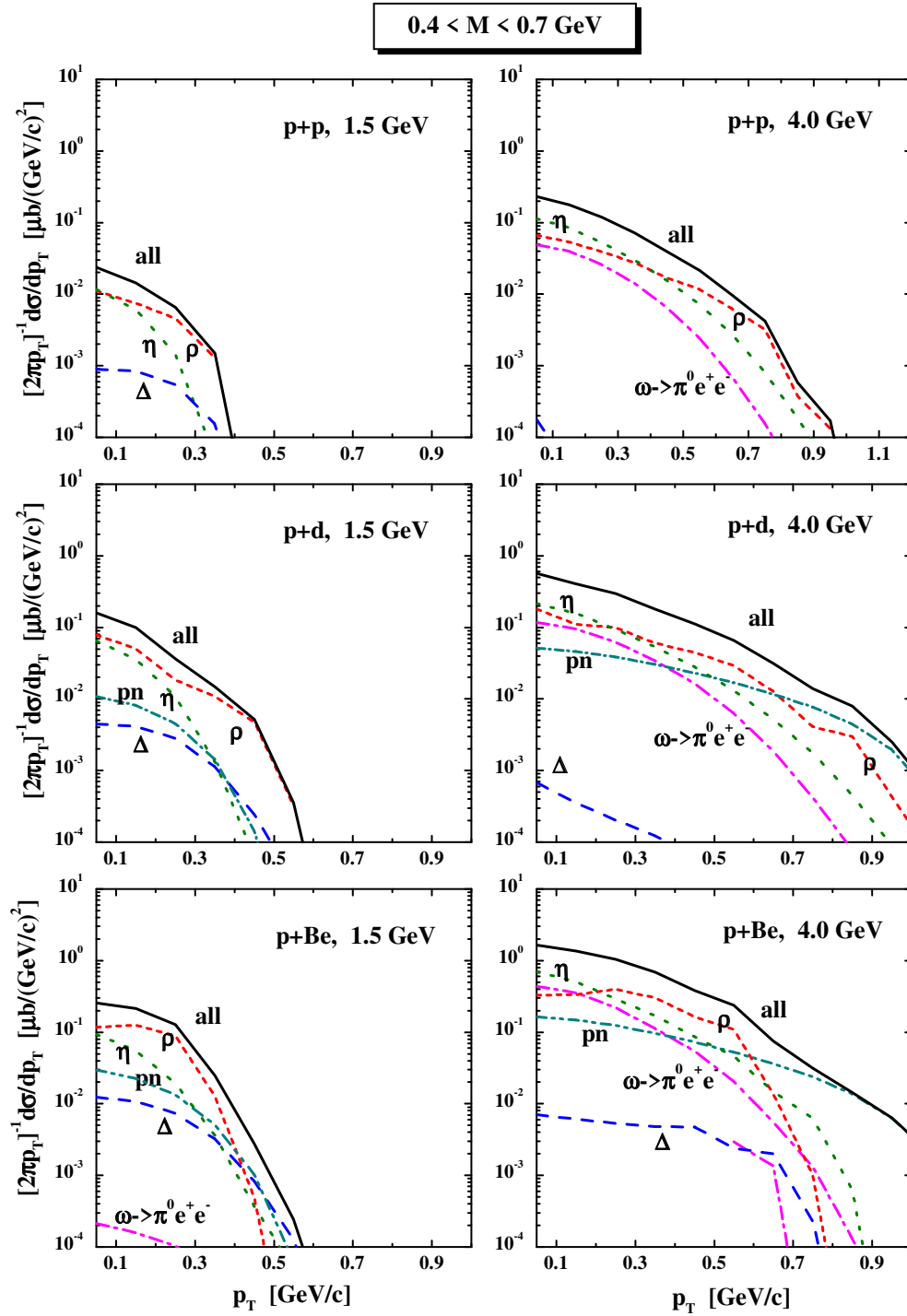


Figure 11: The transverse momentum distribution $d^2\sigma/dp_T d^2p_T = (2\pi p_T)^{-1} d^2\sigma/dp_T$ for pp (upper part), pd (middle part) and pBe collisions (lower part) at 1.5 GeV (left panel) and 4.0 GeV (right panel) implying a cut in invariant mass of $0.4 < M < 0.7 \text{ GeV}$. The assignment of the individual lines is the same as in Figs. 2, 4.

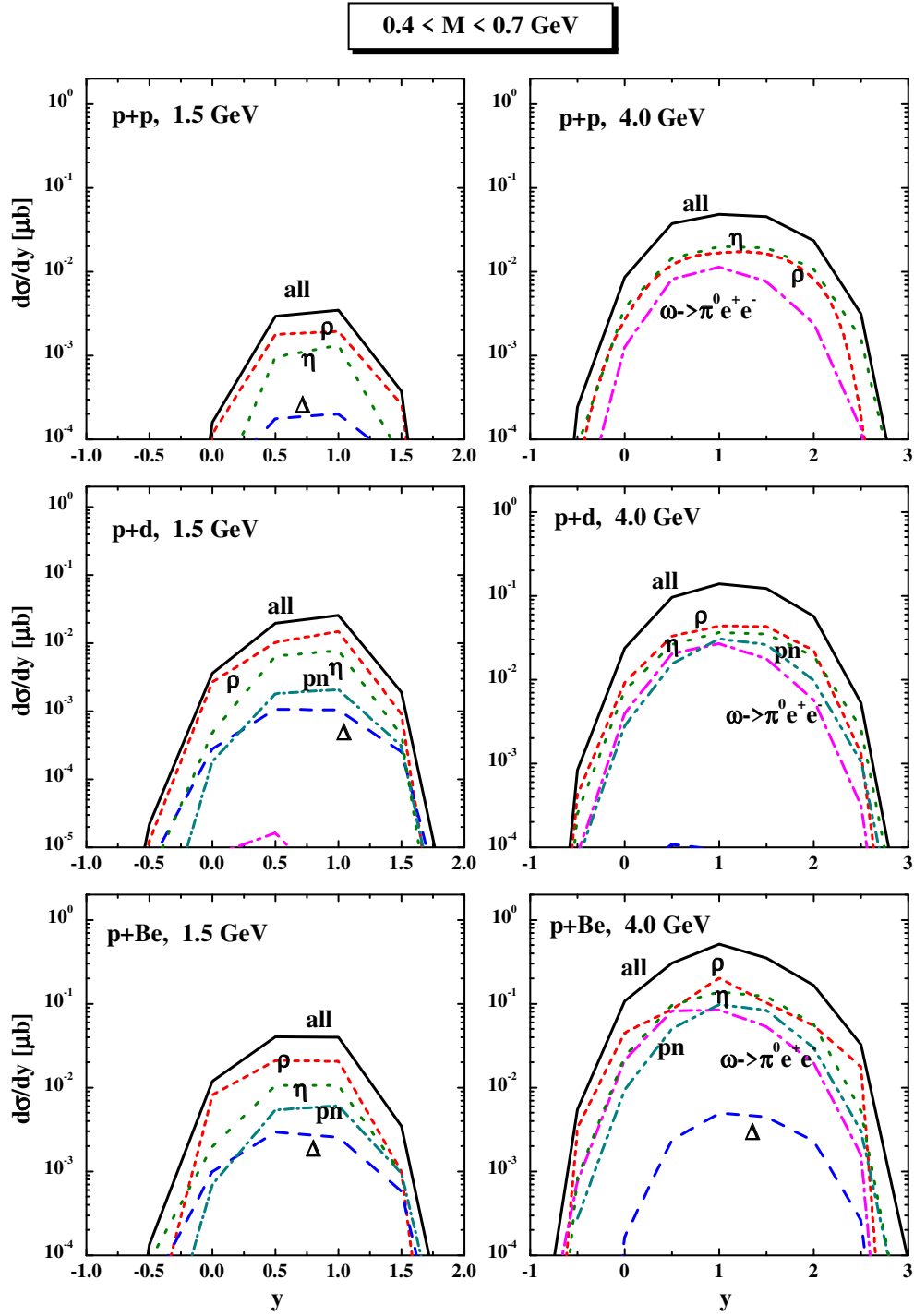


Figure 12: The laboratory rapidity distributions $d\sigma/dy$ for pp (upper part), pd (middle part) and pBe collisions (lower part) at 1.5 GeV (left panel) and 4.0 GeV (right panel) implying a cut in invariant mass of $0.4 < M < 0.7 \text{ GeV}$. The assignment of the individual lines is the same as in Figs. 2, 4.

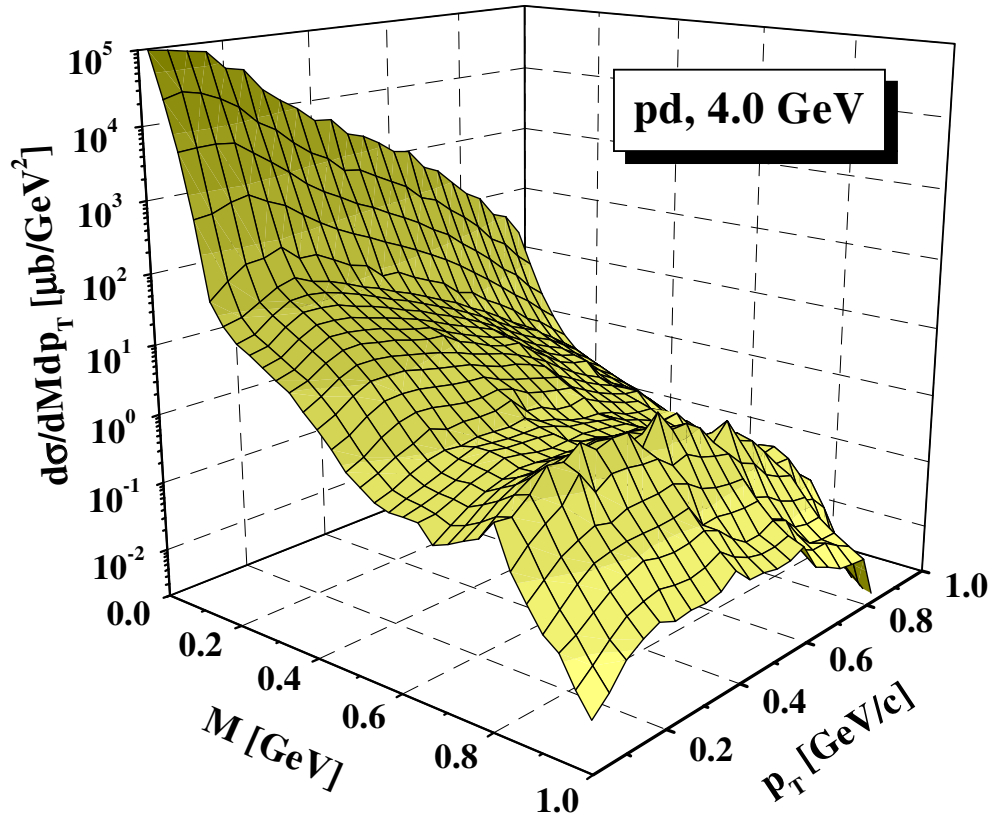


Figure 13: The calculated double differential dilepton spectra $d\sigma/dMdp_T$ as a function of invariant mass M and transverse momentum p_T for pd collisions at 4.0 GeV.